*mathematics*

MDPI

*Article*

# Unsteady Three-Dimensional Flow in a Rotating Hybrid Nanofluid over a Stretching Sheet

**Noor Farizza Haniem Mohd Sohut [1], Siti Khuzaimah Soid [2], Sakhinah Abu Bakar [1] and Anuar Ishak [1,*]**

[1] Department of Mathematical Sciences, Universiti Kebangsaan Malaysia, Bangi 43600, Malaysia; p106827@siswa.ukm.edu.my (N.F.H.M.S.); sakhinah@ukm.edu.my (S.A.B.)
[2] Faculty of Computer and Mathematical Sciences, Universiti Teknologi MARA, Shah Alam 40450, Malaysia; khuzaimah@tmsk.uitm.edu.my
* Correspondence: anuar_mi@ukm.edu.my

**Abstract:** The problem of an unsteady 3D boundary layer flow induced by a stretching sheet in a rotating hybrid nanofluid is studied. A dimensionless set of variables is employed to transform the system of partial differential equations (PDEs) to a set of nonlinear ordinary differential equations (ODEs). Then, the system of ODEs is solved numerically using the MATLAB software. The impacts of different parameters, such as copper nanoparticles volume fraction, radiation, rotation, unsteadiness, and stretching parameters are graphically displayed. It is found that two solutions exist for the flow induced by the stretching sheet. Furthermore, the increasing nanoparticle volume fraction enhances the skin friction coefficient. It is noticed that the skin friction coefficient, as well as the heat transfer rate at the surface, decrease as the rotating parameter increases. Additionally, the thermal radiation as well as the unsteadiness parameter stimulate the temperature.

**Keywords:** unsteady flow; rotation; heat transfer; hybrid nanofluid; stretching sheet; radiation

check for updates

**Citation:** Mohd Sohut, N.F.H.; Soid, S.K.; Abu Bakar, S.; Ishak, A. Unsteady Three-Dimensional Flow in a Rotating Hybrid Nanofluid over a Stretching Sheet. *Mathematics* **2022**, *10*, 348. https://doi.org/10.3390/math10030348

Academic Editors: Camelia Petrescu and Valeriu David

Received: 23 December 2021
Accepted: 22 January 2022
Published: 24 January 2022



## 1. Introduction

The investigation into heat transfer is useful in various engineering applications, such as transpiration cooling, drag reduction, thrust bearing, and radial diffuser design [1]. Usually, fluids are used as heat transporters, such as in heating and cooling processes in transportation systems and industrial processes. It is also noticed that the stretching sheet has gained researchers' attention for years. Researchers have conducted various studies on the physical phenomena and heat transmissions past a stretching plate. It has numerous important applications in industrial production, including the extrusion of plastic sheets, the process of condensation of metallic plates, and glass filer fabrication [2]. The study of flow and heat transfer is of significant importance since the quality of the final product depends on the large extent of the skin friction coefficient and the heat transfer rate at the surface [2]. Recently, the investigation of flow over a stretching sheet has been broadened to many different cases that make the study more interesting. For instance, Shahid et al. [3] studied the effects of swimming gyrotactic microorganisms using Darcy law and Vafai et al. [4] explored the effects of Dufour, Soret, and radiation on the Powell–Eyring fluid flow.

Even though the study of steady-state flows has the greatest practical significance, many scholars are now paying close attention to the study of unsteady-state flows. Steady flow can be defined as a flow in which the fluid characteristics at a given location in the system stay constant throughout time. In contrast, the unsteady flow is defined otherwise, which is time-dependent flow. Sears and Telionis [5] reported the numerical studies of steady and unsteady distinguishing boundary layer flow with Goldstein's type singularities, and a possible comparison between the position of the singularity in relation to the time curves and the point of vanishing wall shear can be made. They discovered a significant difference between vanishing wall shear and separation. The unsteady (transient) boundary layer that is time-varying consists of mostly start-up processes, such as the movements from rest or transitions from one steady-state to another or occasional movements [6]. According to Liao [7], the unsteady flow problem may be resolved in the same manner as the steady-state similarities governed by the nonlinear ODEs. The study found that solving the problem for unsteady flow is as easy as steady flow using the homotopy analysis method (HAM). Suali et al. [8] considered both shrinking and stretching sheets with injection or suction to explore the unsteady flow towards a stagnation point on the sheet. According to this study, the spectrum of dual outcomes rises with mass suction, whereas it reduces with mass injection. The problems related to the unsteady flow can also be found in numerous literature [9–16].

The applications involved the problem of rotating flow, such as flywheels, cutting discs, rotating machinery, computer storage devices, electrical items, and many others [17]. Anuar et al. [18] stated that the fluid flow with a rotating plane was initially introduced by Kármán [19] using the momentum integral method. In the year 1988, Wang [20] explored the rotating fluid flow of the stretching plate. The solutions were determined by the rotation rate parameter, and it was found that the perturbation solutions for small and large rotation rates were comparable to other works of literature. A few years later, Rajeswari and Nath [21] broadened Wang's problem to include the unsteady flow problem by combining the finite-difference scheme with the quasilinearization technique. Takhar et al. [22] have also extended Wang's analysis to include the magnetic field. The application that is related to the present magnetic-rotational model was the chilling process in amalgamation reactors of liquid metal blankets. Yacob et al. [23] investigated a steady rotating flow in a nanofluid containing carbon nanotubes past a stretching/shrinking surface. Carbon nanotubes can be classified into single-walled (SWCNT) and multi-walled (MWCNT). They discovered that the heat transfer enhancement is greater in water-MWCNTs than in water-SWCNTs. Moreover, recent studies in this area may be found in references [24–27].

Nanofluid is a new amalgamation formed, as stated by Choi [28]. A nanofluid is formed by adding tiny particles in nano-dimensions to the base fluid. Nanofluids have higher thermal conductivity and are more effective in heat transport activities compared to their base fluid. Hence, it is also well acknowledged and accepted empirically and conceptually that dispersing nanoparticles in a liquid may improve the liquid's thermo-physical properties [29]. Nanotechnology has advanced rapidly in recent years, and by combining many nanoparticle elements, stability issues and low heat conductivity can be addressed. Nanofluids will save energy, improve thermal efficiency, speed up processes, and increase the life of the equipment. Using a finite element simulation, Rana et al. [24] observed the unsteady magnetohydrodynamic (MHD) boundary layer rotating nanofluid flow on a stretching plate. Apart from that, nanofluid provides a number of advantages, including less component degradation and blockage in tiny channels than fluid containing micro-to millimeter-sized particles in suspension [30]. Similar problems in nanofluid but with different approaches were published by Ghadimi et al. [31], Noor et al. [32], Ahmad et al. [33], and Khan et al. [34].

Due to its importance in providing greater properties than nanofluid, hybrid nanofluid has recently been a topic of discussion. It's employed in heat transfer applications using particles that are less than 100 nanometers in size. Higher energy efficiency, lower operating costs, and greater performance are among the contributions of the high thermal conductivity of a hybrid nanofluid [35]. Hybrid nanofluids have recently piqued the curiosity of many academics as a novel technological idea. Using a two-step technique, Suresh et al. [36] studied the combination of $Al_2O_3$-$Cu/H_2O$ hybrid nanofluid. They found that the distinct nanoparticles improved the parameters of the hybrid nanofluid. Later, Suresh et al. [37] discussed the heat transport and the impacts of the alumina-copper/$H_2O$ hybrid nanofluid. Numerical research of the 3D hybrid nanofluid flux with Newtonian heating and Lorentz force effects on a stretching plate was conducted by Devi and Devi [38]. Later, they continued the investigation across a stretching plate on increasing heat transmission in a copper-alumina/$H_2O$ hybrid nanofluid [35].

Moreover, Waini et al. [39] investigated the unsteady hybrid nanofluid flow and heat transmission through a stretching, as well as a shrinking surface. For a particular unsteadiness parameter range, dual solutions exist; the results demonstrate that increasing the nanoparticle volume percentage of Cu for the first solution will improve the skin friction coefficient, while the second solutions show the opposite. Furthermore, the unsteady hybrid nanofluid flow on a porous biaxial stretching or shrinking plate, the effects of buoyancy and stagnation flow on an exponentially stretching or shrinking vertical plate, heat transfer, and MHD flow over a porous stretching/shrinking wedge, as well as the flow past a permeable non-isothermal shrinking surface were reviewed by Waini et al. [40–43]. The stability analysis was conducted by Zainal et al. [44] for the unsteady 3D magnetohydrodynamic hybrid nanofluid for Homann flow. Hayat and Nadeem [45] described how heat dissipation might be improved using Ag-CuO/$H_2O$ hybrid nanofluid. Later, Hayat et al. [26] extended the study of rotational flow with partial slip and radiation effects. Subsequently, Anuar et al. [18] explored copper-alumina/water hybrid nanofluid with radiation on a rotating surface. They reported the stability of the solutions over time. The study of hybrid nanofluid flows has been diversified by Khan et al. [46] to various nanoparticle shape factors and for different base fluids.

Motivated by the earlier studies on rotating hybrid nanofluids, the present work intends to explore the rotation and radiation impacts on the unsteady 3D rotating flow of a hybrid nanofluid over a stretching sheet. The boundary value problem is solved numerically using the MATLAB software. The model is adopted from Rana et al. [24] and Devi and Devi [35], where the hybrid nanofluid $Al_2O_3$-Cu/$H_2O$ is considered in this study. Rana et al. [24] studied the unsteady magnetohydrodynamic flow on a stretching sheet in a rotating nanofluid. The influences of the related parameters are visually depicted, and the numerical findings obtained are compared with the existing literature. The novelty of this study can also be seen in the discovery of dual solutions when the surface of the sheet is stretched. This discovery also has applications in a variety of sectors of science and technology, and it is useful for engineers as well as scientists to understand the behavior of the boundary layer flow.

## 2. Problem Formulation

The unsteady rotating flow of a hybrid nanofluid on a stretching sheet is considered as demonstrated in Figure 1, where $(x, y, z)$ are cartesian coordinates with the sheet at $z = 0$. The stretching velocities in the $x$ and $y$ directions are denoted by $u_w(x,t)$ and $v_w(x,t)$, respectively, while $\omega$ is the uniform angular velocity of the rotation, see Figure 1. Moreover, the ambient temperature of the fluid is $T_\infty$ and the sheet temperature is $T_w$. The hybrid nanofluid $Al_2O_3$-Cu/$H_2O$ is considered in this study. The desired hybrid nanofluid is formed by scatting copper nanoparticles in water to create Cu-$H_2O$ nanofluid, and then aluminum oxide nanoparticles are added into that Cu-$H_2O$ nanofluid.

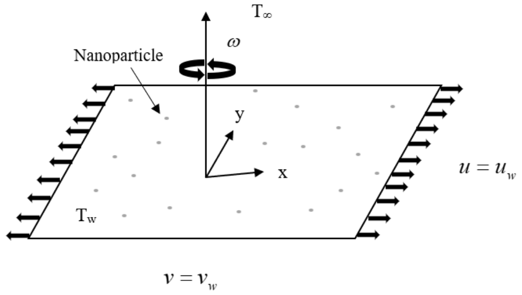


**Figure 1.** Physical configuration.

The governing equations are adopted from Refs. [2,20,21,25], and may be written as

$$\frac{\partial u}{\partial x} + \frac{\partial v}{\partial y} + \frac{\partial w}{\partial z} = 0 \tag{1}$$

$$\frac{\partial u}{\partial t} + u\frac{\partial u}{\partial x} + v\frac{\partial u}{\partial y} + w\frac{\partial u}{\partial z} = 2\omega v + \frac{\mu_{hnf}}{\rho_{hnf}}\frac{\partial^2 u}{\partial z^2} \tag{2}$$

$$\frac{\partial v}{\partial t} + u\frac{\partial v}{\partial x} + v\frac{\partial v}{\partial y} + w\frac{\partial v}{\partial z} = -2\omega u + \frac{\mu_{hnf}}{\rho_{hnf}}\frac{\partial^2 v}{\partial z^2} \tag{3}$$

$$\frac{\partial w}{\partial t} + u\frac{\partial w}{\partial x} + v\frac{\partial w}{\partial y} + w\frac{\partial w}{\partial z} = \frac{\mu_{hnf}}{\rho_{hnf}}\frac{\partial^2 w}{\partial z^2} \tag{4}$$

$$\frac{\partial T}{\partial t} + u\frac{\partial T}{\partial x} + v\frac{\partial T}{\partial y} + w\frac{\partial T}{\partial z} = \frac{k_{hnf}}{(\rho C_p)_{hnf}}\frac{\partial^2 T}{\partial z^2} - \frac{1}{(\rho C_p)_{hnf}}\frac{\partial q_r}{\partial z} \tag{5}$$

The boundary conditions are

$$\begin{array}{ll} u = u_w(x,t) = \frac{cx}{1-\alpha t}, \quad v = 0, \quad w = 0, \quad T = T_w & \text{at } z = 0 \\ u \to 0, \quad v \to 0, \quad T \to T_\infty & \text{as} \quad z \to \infty \end{array} \tag{6}$$

where $(u, v, w)$ are the velocity components along the $(x, y, z)$ directions, $t$ refers to time, $T$ is the fluid temperature, $c > 0$ for the stretching sheet and $q_r$ is the radiative heat flux, $k_{hnf}$ is the thermal conductivity, $\mu_{hnf}$ is the dynamic viscosity, $\rho_{hnf}$ is the density, $(\rho C_p)_{hnf}$ is the heat capacity, and $\sigma_{hnf}$ is the electrical conductivities. The thermophysical properties are given in [47] as presented in Table 1.

**Table 1.** Thermophysical properties.

| Properties | Hybrid Nanofluid |
|---|---|
| Density | $\rho_{hnf} = \phi_{Al_2O_3}\rho_{Al_2O_3} + \phi_{Cu}\rho_{Cu} + \left(1 - \phi_{hnf}\right)\rho_f$ |
| Dynamic viscosity | $\mu_{hnf} = \mu_f(1 - \phi_{Al_2O_3} - \phi_{Cu})^{-2.5}$ |
| Thermal conductivity | $\frac{k_{hnf}}{k_f} = \left\{\frac{\phi_{Al_2O_3}k_{Al_2O_3}+\phi_{Cu}k_{Cu}}{\phi_{Al_2O_3}+\phi_{Cu}} + 2k_f + 2(\phi_{Al_2O_3}k_{Al_2O_3} + \phi_{Cu}k_{Cu}) - 2(\phi_{Al_2O_3} + \phi_{Cu})k_f\right\} \times \left\{\frac{\phi_{Al_2O_3}k_{Al_2O_3}+\phi_{Cu}k_{Cu}}{\phi_{Al_2O_3}+\phi_{Cu}} + 2k_f - (\phi_{Al_2O_3}k_{Al_2O_3} + \phi_{Cu}k_{Cu}) + (\phi_{Al_2O_3} + \phi_{Cu})k_f\right\}^{-1}$ |
| Heat capacity | $(\rho C_p)_{hnf} = \phi_{Al_2O_3}(\rho C_p)_{Al_2O_3} + \phi_{Cu}(\rho C_p)_{Cu} + \left(1 - \phi_{hnf}\right)(\rho C_p)_f$ |

Where $\phi_{hnf} = \phi_{Al_2O_3} + \phi_{Cu}$.

In Table 1, $\phi$ denotes the nanoparticle volume fraction where $\phi = 0$ indicates the regular fluid, $\phi_{Al_3O_2}$ correlates to $Al_2O_3$, and $\phi_{Cu}$ correlates to Cu. The physical properties of the nanoparticles and the base fluid are given in Table 2, as reported in [48].

**Table 2.** Thermophysical properties of nanoparticles and water (base liquid).

| Physical Properties | $Al_2O_3$ | Cu | Water |
|---|---|---|---|
| $C_p(\mathrm{J/KgK})$ | 765 | 385 | 4179 |
| $\rho\left(\mathrm{kg/m^3}\right)$ | 3970 | 8933 | 997.1 |
| $k(\mathrm{W/mK})$ | 40 | 400 | 0.613 |
| $\beta \times 10^{-5}(1/\mathrm{K})$ | 0.85 | 1.67 | 21 |

Following Bataller [49], Ishak [50], Magyari and Pantokratoras [51], and Roşca, Roşca and Pop [52], the Rosseland approximation is applied to exhibit $q_r$ as

$$q_r = -\frac{4}{3}\frac{\sigma^*}{k^*}\frac{\partial T^4}{\partial y} \tag{7}$$

where $q_r$, $k^*$ and $\sigma^*$ respectively indicate the radiative heat flux, mean absorption coefficient, and the Stefan–Boltzmann constant. By neglecting higher-order terms and employing the

Taylor series, $T^4$ may be approximated as $T^4 \approx 4T_\infty^3 T - 3T_\infty^4$. Equation (5) is now may be written as

$$\frac{\partial T}{\partial t} + u\frac{\partial T}{\partial x} + v\frac{\partial T}{\partial y} + w\frac{\partial T}{\partial z} = \frac{1}{(\rho C_p)_{hnf}}\left(k_{hnf} + \frac{16\sigma^* T_\infty{}^3}{3k^*}\right)\frac{\partial^2 T}{\partial z^2} \tag{8}$$

The given transformation variables are according to Maqsood et al. [25],

$$\begin{gathered} u = \frac{ax}{1-\alpha t}f'(\eta), \qquad v = \frac{ax}{1-\alpha t}h(\eta), \qquad w = -\sqrt{\frac{a\nu_f}{1-\alpha t}}f(\eta) \\ \theta(\eta) = \frac{T-T_\infty}{T_w-T_\infty}, \qquad \eta = z\sqrt{\frac{a/\nu_f}{1-\alpha t}} \end{gathered} \tag{9}$$

where $(')$ denotes differentiation w.r.t. $\eta$, $a > 0$ is the stretching constant along the $x$ direction, $\alpha$ is a parameter indicating the flow unsteadiness, $\nu_f$ is the kinematic viscosity of the base fluid, and the nonlinear rotating angular velocity is $\omega = \omega^*/(1-\alpha t)$.

Substituting the similarity variables (9) into Equations (1)–(4) and (8) yields

$$\frac{\mu_{hnf}/\mu_f}{\rho_{hnf}/\rho_f}f''' + ff'' - f'^2 + 2\Omega h - \beta\left(f' + \frac{\eta}{2}f''\right) = 0 \tag{10}$$

$$\frac{\mu_{hnf}/\mu_f}{\rho_{hnf}/\rho_f}h'' + fh' - f'h - 2\Omega f' - \beta\left(h + \frac{\eta}{2}h'\right) = 0 \tag{11}$$

$$\frac{1}{\Pr}\frac{1}{(\rho C_p)_{hnf}/(\rho C_p)_f}\left(\frac{k_{hnf}}{k_f} + \frac{4}{3}Rd\right)\theta'' + f\theta' - \beta\frac{\eta}{2}\theta' = 0 \tag{12}$$

The boundary conditions are as follows:

$$\begin{array}{llll} f(0) = 0, & f'(0) = \lambda, & h(0) = 0, & \theta(0) = 1 \\ f'(\eta) \to 0, & h(\eta) \to 0, & \theta(\eta) \to 0 & \text{as } \eta \to \infty \end{array} \tag{13}$$

where $\Omega$ is the rotation parameter, $\beta$ the unsteadiness parameter, Pr indicates the Prandtl number, $Rd$ the radiation parameter, and $\lambda > 0$ is the stretching parameter respectively defined as

$$\Omega = \frac{\omega^*}{a}, \qquad \beta = \frac{\alpha}{a}, \qquad \Pr = \frac{\nu_f}{\alpha_f}, \qquad Rd = \frac{4\sigma^* T_\infty{}^3}{k^* k_f}, \qquad \lambda = \frac{c}{a} \tag{14}$$

It is noted that $\lambda > 0$ is for stretching sheet, $\lambda < 0$ for shrinking sheet, and $\lambda = 0$ corresponds to static sheet.

We notice that the regular fluid $\left(\phi_{Al_2O_3} = \phi_{Cu} = 0\right)$ and the absence of rotating parameter $(\Omega = 0)$, Equation (10) becomes Equation (15) which is consistent with Equation (6) as in Fang et al. [53].

$$f''' + ff'' - f'^2 - \beta\left(f' + \frac{\eta}{2}f''\right) = 0 \tag{15}$$

The quantities of physical interest are the skin friction coefficients and the local Nusselt number which are given as follows:

$$\begin{gathered} C_{fx} = \frac{\mu_{hnf}}{\rho_f u_e{}^2(x)}\left(\frac{\partial u}{\partial z}\right)_{z=0}, \qquad C_{fy} = \frac{\mu_{hnf}}{\rho_f u_e{}^2(x)}\left(\frac{\partial v}{\partial z}\right)_{z=0}, \\ Nu_x = -\frac{xk_{hnf}}{k_f(T_f - T_\infty)}\left(\frac{\partial T}{\partial z}\right)_{z=0} + x(q_r)_{z=0} \end{gathered} \tag{16}$$

Using Equations (10) and (17) yields

$$\begin{gathered} \mathrm{Re}_x{}^{1/2}C_{fx} = \frac{\mu_{hnf}}{\mu_f}f''(0), \qquad \mathrm{Re}_x{}^{1/2}C_{fy} = \frac{\mu_{hnf}}{\mu_f}h'(0), \\ \mathrm{Re}_x{}^{-1/2}Nu_x = -\left(\frac{k_{hnf}}{k_f} + \frac{4}{3}Rd\right)\theta'(0) \end{gathered} \tag{17}$$

where $\mathrm{Re}_x$ is the local Reynolds number defined as $\mathrm{Re}_x = u_e(x)x/\nu_f$.

## 3. Results and Discussion

The governing non-linear ordinary differential equations (ODEs) (10)–(12) subjected to the boundary conditions (13) are solved numerically using the built-in function "bvp4c" available in the MATLAB software. The detailed settings are described in [54]. The validation for the skin friction coefficient in $x$ and $y$ directions $f''(0)$ and $h'(0)$, respectively, is obtained, which agrees with Wang [20], Nazar et al. [2], and Rana et al. [24]. The comparisons are for the stretching surface, $\lambda = 1$ in the absence of solid volume fraction $(\phi_1 = \phi_2 = 0)$ at a steady state for different values of $\Omega$ as presented in Table 3. For convenient purposes, the subscripts '1' and '2' indicate the alumina ($Al_2O_3$) and the copper (Cu), respectively.

**Table 3.** Comparison of $f''(0)$ and $h'(0)$ for $\beta = 0$, $\lambda = 1$ and variation of $\Omega$.

| $\Omega$ | Wang [20] | | Nazar et al. [2] | | Rana et al. [24] | | Present Study | |
|---|---|---|---|---|---|---|---|---|
| | $f''(0)$ | $h'(0)$ | $f''(0)$ | $h'(0)$ | $f''(0)$ | $h'(0)$ | $f''(0)$ | $h'(0)$ |
| 0 | −1 | 0 | −1 | 0 | −1 | 0 | −1 | 0 |
| 0.5 | −1.1384 | −0.5128 | −1.1384 | −0.5128 | −1.1384 | −0.5128 | −1.1384 | −0.5128 |
| 1.0 | −1.3250 | −0.8371 | −1.3250 | −0.8371 | −1.3250 | −0.8371 | −1.3250 | −0.8371 |
| 2.0 | −1.6523 | −1.2873 | −1.6523 | −1.2873 | −1.6523 | −1.2873 | −1.6523 | −1.2873 |
| 5.0 | - | - | - | - | −2.3903 | −2.1502 | −2.3903 | −2.1502 |

The effects of non-dimensional parameters like Cu nanoparticle volume fraction $\phi_2$, rotating parameter $\Omega$, radiation parameter $Rd$, and unsteadiness parameter $\beta$, are discussed and illustrated in Figures 2–9. We can see from these diagrams that there are two solutions within the first and second solutions when $\lambda > 0$. The solutions are found up to a specific critical value $\lambda = \lambda_c$.

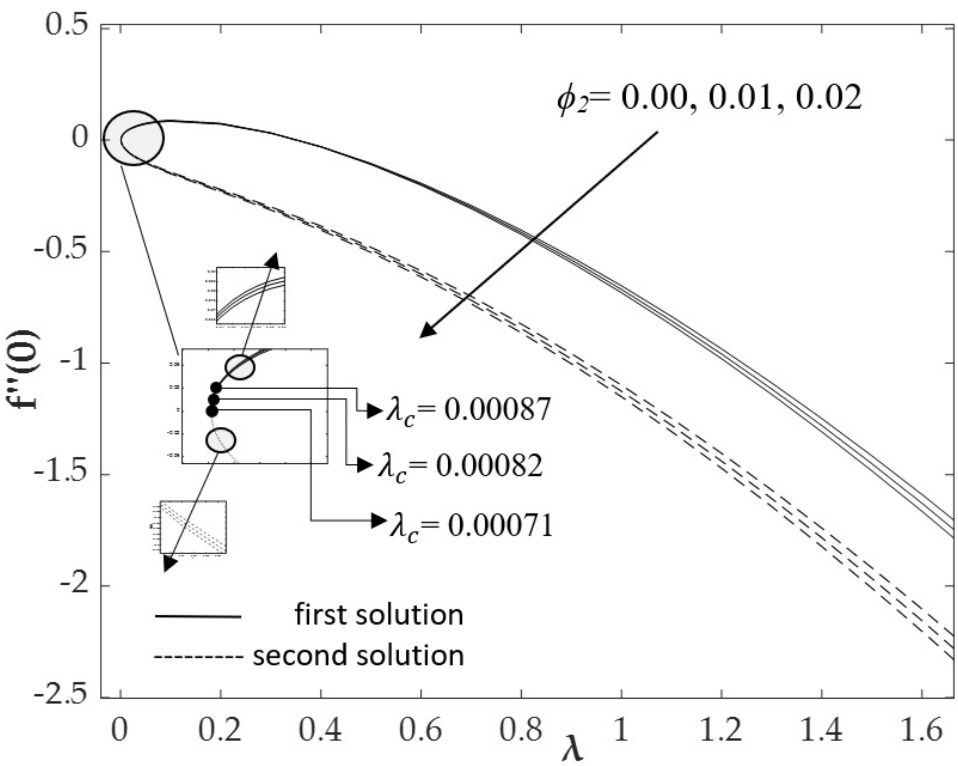


**Figure 2.** Variations of the skin friction coefficient in the $x$ direction, $f''(0)$, with stretching parameter $\lambda$ for various values of $\phi_2$.

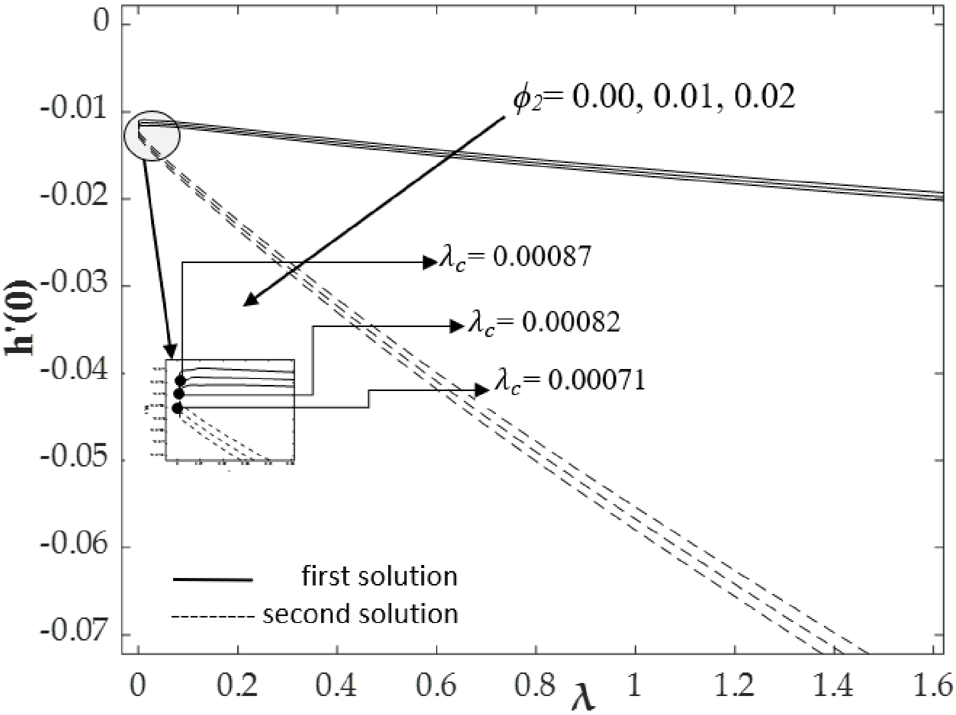


**Figure 3.** Variations of the skin friction coefficient in the $y$ direction, $h'(0)$, with stretching parameter $\lambda$ for various values of $\phi_2$.

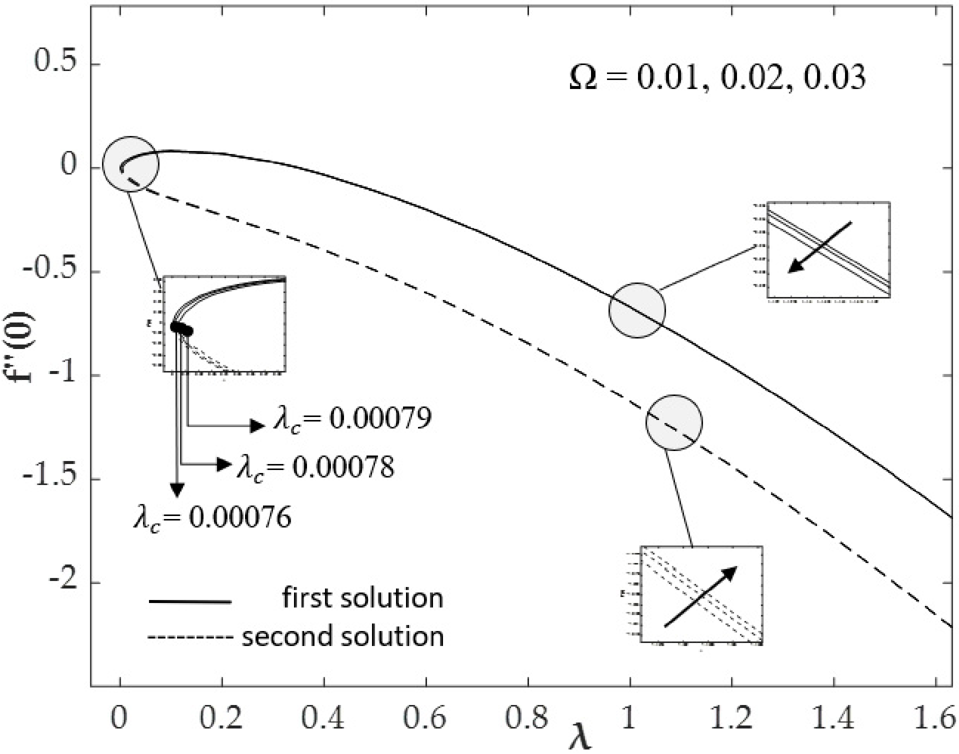


**Figure 4.** Variations of the skin friction coefficient in the $x$ direction, $f''(0)$, with stretching parameter $\lambda$ for various values of $\Omega$.

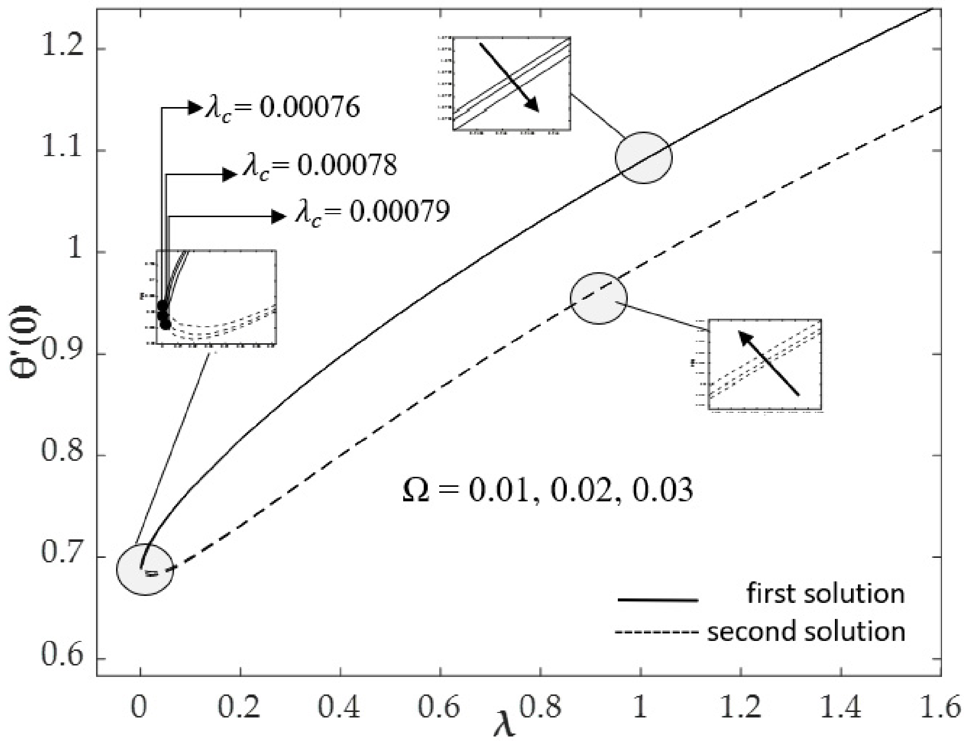


**Figure 5.** Variations of the local Nusselt number$-\theta'(0)$with stretching parameter $\lambda$ for different values of $\Omega$.

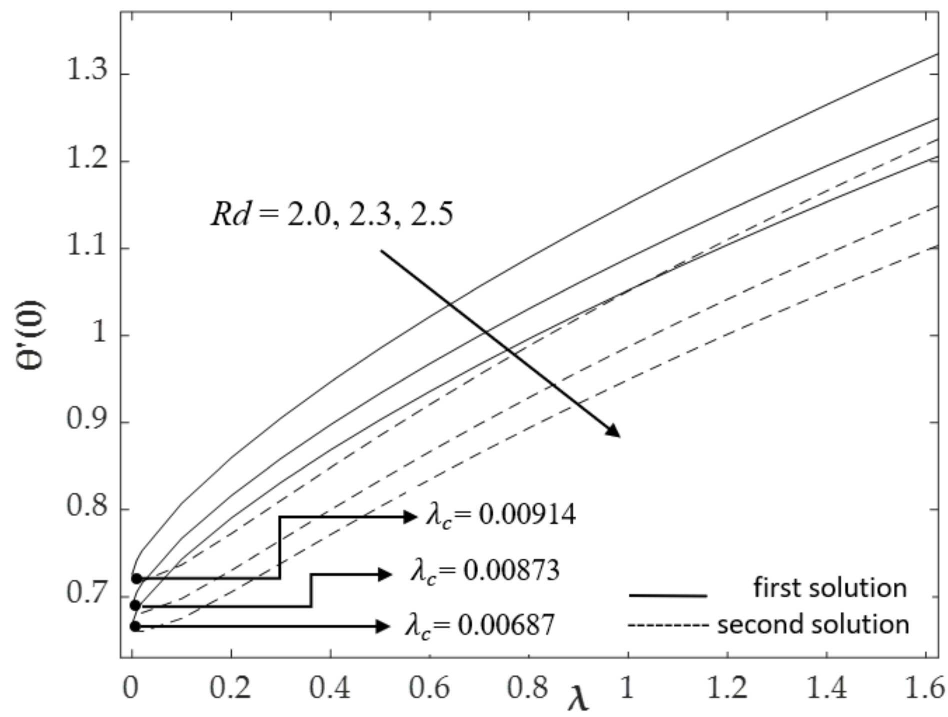


**Figure 6.** Variations of the local Nusselt number$-\theta'(0)$ with stretching parameter $\lambda$ for different values of *Rd*.

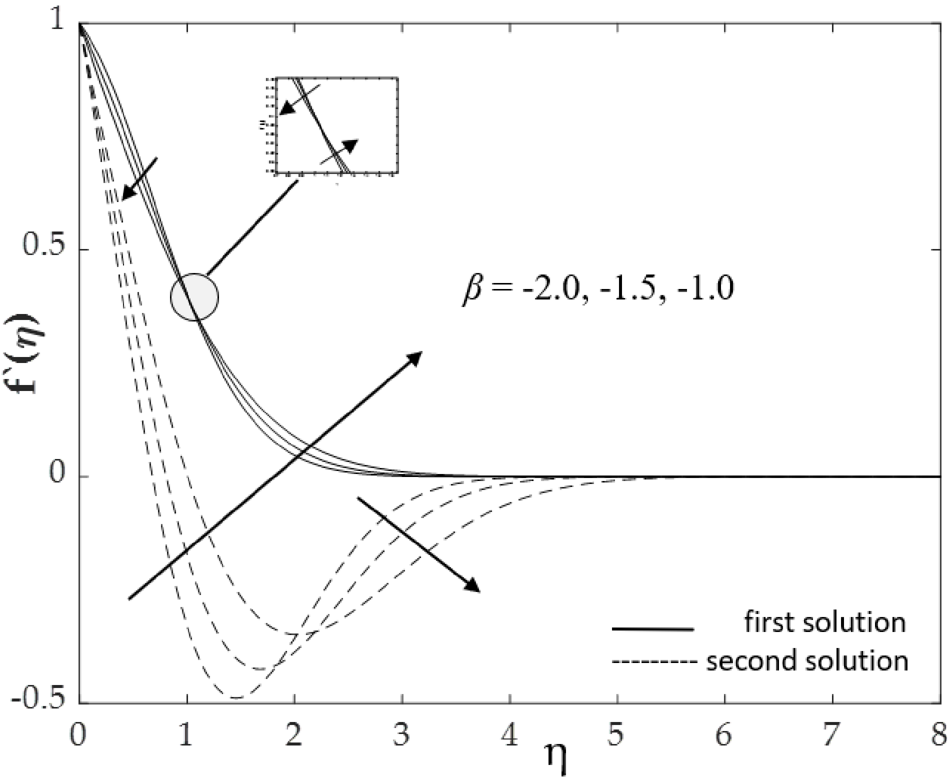


**Figure 7.** Velocity profiles in the $x$ direction $f'(\eta)$, for different values of $\beta$ when $Rd = 2.3$, $\lambda = 1$, $\phi_1 = \phi_2 = 0.01$, $\Pr = 6.2$ and $\Omega = 0.01$.

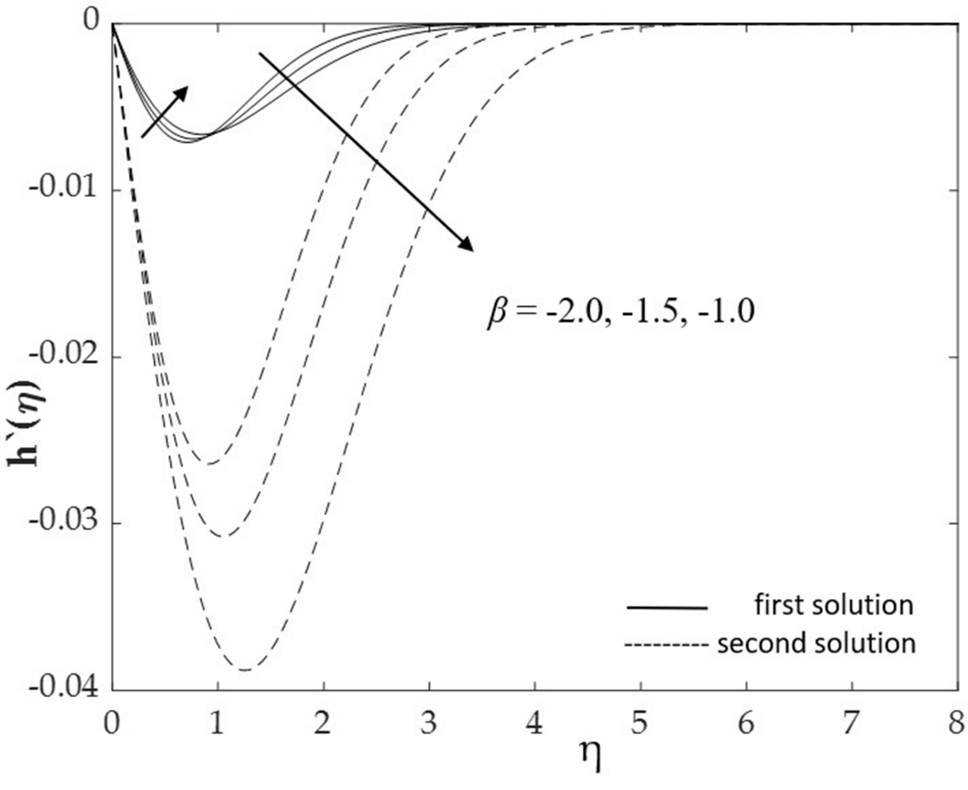


**Figure 8.** Velocity profiles in the $y$ direction $h(\eta)$, for different values of $\beta$ when $Rd = 2.3$, $\lambda = 1$, $\phi_1 = \phi_2 = 0.01$, $\Pr = 6.2$ and $\Omega = 0.01$.

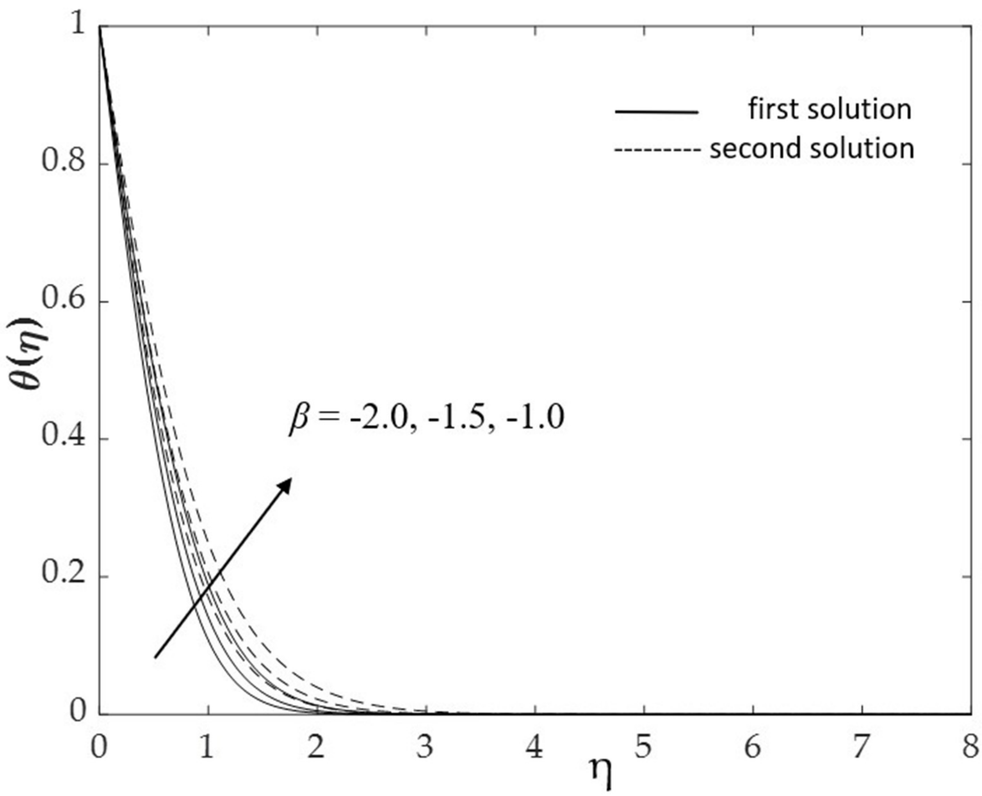


**Figure 9.** Temperature distribution $\theta(\eta)$ for different values of $\beta$ when $\mathrm{Pr} = 6.2$, $Rd = 2.3$, $\lambda = 1$, $\phi_1 = \phi_2 = 0.01$ and $\Omega = 0.01$.

Figures 2 and 3 depict the changes in the skin friction $f''(0)$ in the $x$ direction and $h'(0)$ in the $y$ direction, respectively, for the various values of $\phi_2$ when $\mathrm{Pr} = 6.2$, $Rd = 2.3$, $\beta = -1$, $\phi_1 = 0.01$ and $\Omega = 0.01$. It is discovered that as the Cu nanoparticle volume fraction $\phi_2$ increases, the values of $f''(0)$ and $h'(0)$ decrease (increase in absolute sense) for both solutions. There are two solutions for a particular range of stretching strength $\lambda > 0$. It is noted that the critical value $\lambda_c$ for Cu/$H_2O$ nanofluid ($\phi_1 = 0.01,\ \phi_2 = 0.00$) is 0.00087 and for the hybrid nanofluid $Al_2O_3$-Cu/$H_2O$ ($\phi_1 = 0.01,\ \phi_2 = 0.01,\ 0.02$) are 0.00082 and 0.00071, respectively. It is found that the critical values $\lambda_c$ decrease when the values of $\phi_2$ increase. When compared to the nanofluid, the hybrid nanofluid has a higher concentration of nanoparticles. In particular, a higher concentration of nanoparticles will lead to the boundary layer separation being delayed. In Figure 2, the magnitude of $f''(0)$ rises in perfect sync with the Cu nanoparticle volume fraction $\phi_2$. It is noted that the solid surface exerts a drag force on the fluid for negative values of $f''(0)$. Meanwhile, if the stretching strength is less $(0.05 < \lambda < 0.4)$, it has the opposite behavior, in which the fluid exerts a drag force on the sheet, represented by positive values of $f''(0)$. The solution exists up to the critical values of λ as shown in Figure 2, where $\lambda_c$ = 0.00087, 0.00082, and 0.00071 for Cu nanoparticle volume fraction parameter $\phi_2$ =0.00, 0.01, and 0.02, respectively. It is noted that there are positive and negative values of $f''(0)$. The positive values indicate a drag force imposed by the fluid on the solid surface, while the negative sign implies a drag force imposed by the solid surface on the fluid. On the other hand, the case $f''(0) = 0$ indicates that the fluid-solid contact is free of friction moving at the same velocity. Overall, the higher the ratio of stretching, the higher the drag force on the surface. There are significant effects on the second solution in Figure 3, where the $y$-direction skin friction coefficient, $h'(0)$ is always negative for $\lambda > 0$ as the drag force is dominant on the solid surface. The effects of drag force in the $y$ direction are less than the effects in the $x$ direction.

In addition, Figures 4 and 5 elucidate the variation in the skin friction $f''(0)$ in the $x$ direction and heat transfer $-\theta'(0)$ for various values of the rotating parameter $\Omega$ when

$\Pr = 6.2$, $Rd = 2.3$, $\beta = -1$, and $\phi_1 = \phi_2 = 0.01$. It is observed that the critical values $\lambda_c$ are getting bigger with the increasing values of the rotating parameter $\Omega$. The critical values of $\lambda$ for the rotating parameter $\Omega = 0.01$, 0.02, and 0.03 are $\lambda_c$ =0.00076, 0.00078, and 0.00079, respectively. The increment values of the rotating parameter depend on the rotation rate, as well as the stretching rate [25]. Figure 4 shows that $f''(0)$ decreases as $\Omega$ increases for the first solution, but it increases for the second solution, which is consistent with the results presented in Figure 2. Even though the gap is small, due to the small variation of the rotating parameter $\Omega$, but the existence of the dual solutions can still be seen. However, Figure 5 shows the opposite results, where for the first solution, increasing $\Omega$ leads to a decrease in the heat transfer rate $-\theta'(0)$, while for the second solution, it rises.

The variations of heat transfer rate $-\theta'(0)$ with $\lambda$ for various values of radiation parameter $Rd$ when $\Pr = 6.2$, $\Omega = 0.01$, $\beta = -1$, and $\phi_1 = \phi_2 = 0.01$ are presented in Figure 6. We note that as $Rd$ increases, the absolute value of $-\theta'(0)$ decreases. The critical values, $\lambda_c = 0.00914$, 0.00873, and 0.00687 for $Rd$ =2.0, 2.3, and 2.5, respectively, are also presented in this figure. It is noted that $Rd$ gives no effect on the skin friction coefficients for both the $x$ and $y$ directions, which is expected since the velocity field is not affected by the thermal field, see Equations (10)–(13).

Figures 7–9 elucidate the effects of the unsteadiness parameter $\beta$ on the fluid velocity in the $x$ and $y$ directions, as well as the fluid temperature. Initially, by increasing $\beta$, the velocity of the first solution decreases, while the velocity of the second solution increases. However, the opposite behavior is seen in the velocity in the $y$ direction. When the fluid moves towards inviscid flow, the directional movement of the velocity changes in the $x$ direction for first and second solutions, while the movement of velocity in the $y$ direction is consistent with decreasing towards the quiescent fluid. These scenarios imply thickening of the velocity boundary layer. In addition, the temperature increases for both solutions. It shows a consistent analysis that the thermal boundary layer thickness is also rising.

## 4. Conclusions

The problem of the unsteady 3D rotating hybrid nanofluid flow on a stretching sheet was explored. The governing PDEs were transformed to ODEs using a suitable similarity transformation. The effects of the involved parameters on the physical quantities of interest were visually shown and analyzed. The existence of double solutions was discovered for the stretching situation. In addition, the higher concentration of the nanoparticle volume fraction slowed down the boundary layer flow separation. The function $h(\eta)$ was found to be negative, which explains that the counterclockwise fluid rotation influences the fluid flow in the negative $y$ direction. The positive skin friction coefficient shows that the fluid imposes a drag force on the solid surface, while the negative value implies the contrary. The results showed that the radiation parameter, $Rd$, emits the heat energy into the boundary layer, thus leading to a temperature rise of the hybrid nanofluid and subsequently enhancing the heat transfer rate of the fluid.

**Author Contributions:** Writing—original draft, N.F.H.M.S.; methodology, N.F.H.M.S., S.K.S.; generating numerical results, N.F.H.M.S., S.K.S.; validation, S.A.B., A.I.; writing—review and editing, S.A.B., A.I.; supervising, S.K.S., S.A.B., A.I.; funding acquisition, A.I. All authors have read and agreed to the published version of the manuscript.

**Funding:** This research was funded by Universiti Kebangsaan Malaysia (DIP-2020-001).

**Institutional Review Board Statement:** Not applicable.

**Informed Consent Statement:** Not applicable.

**Conflicts of Interest:** The authors declare no conflict of interest.

## Nomenclature

| | |
|---|---|
| $a, c$ | constants |
| $C_\infty$ | ambient concentration |
| $C_f$ | skin friction coefficient |
| $C_p$ | specific heat at constant pressure ($\text{Jkg}^{-1}\text{K}^{-1}$) |
| $(\rho C_p)$ | heat capacitance of the fluid ($\text{JK}^{-1}\text{m}^{-3}$) |
| $f'$ | velocity in the $x$-direction |
| $h$ | velocity in the $y$-direction |
| $k$ | thermal conductivity of the fluid ($\text{Wm}^{-1}\text{K}^{-1}$) |
| $k^*$ | Rosseland mean absorption coefficient ($\text{m}^{-1}$) |
| $Nu_x$ | local Nusselt number |
| Pr | Prandtl number |
| $q_r$ | radiative heat flux ($\text{Wm}^{-2}$) |
| $Rd$ | radiation parameter |
| $\text{Re}_x$ | local Reynolds number |
| $t$ | time ($s$) |
| $T$ | fluid temperature (K) |
| $T_\infty$ | ambient temperature (K) |
| $T_w$ | surface temperature (K) |
| $u, v, w$ | velocity component in the $x$-, $y$- and $z$- directions ($\text{ms}^{-1}$) |
| $u_w$ | velocity in the $x$ direction ($\text{ms}^{-1}$) |
| $v_w$ | velocity in the $y$ direction ($\text{ms}^{-1}$) |
| $x, y, z$ | Cartesian coordinates (m) |
| **Greek Symbols** | |
| $\alpha$ | a parameter indicates the flow unsteadiness |
| $\beta$ | unsteadiness parameter |
| $\eta$ | similarity variable |
| $\theta$ | dimensionless temperature |
| $\lambda$ | stretching parameter |
| $\mu$ | dynamic viscosity ($\text{kgm}^{-1}\text{s}^{-1}$) |
| $\nu$ | kinematic viscosity of the fluid ($\text{m}^2\text{s}^{-1}$) |
| $\rho$ | density of the fluid ($\text{kgm}^{-3}$) |
| $\sigma$ | electric conductivity ($\text{Sm}^{-1}$) |
| $\sigma^*$ | Stefan-Boltzmann constant ($\text{Wm}^{-2}\text{K}^{-4}$) |
| $\phi$ | nanoparticle volume fraction |
| $\Omega$ | rotating parameter |
| $\omega$ | angular velocity (rad $\text{s}^{-1}$) |
| **Subscripts** | |
| $f$ | base fluid |
| $hnf$ | hybrid nanofluid |
| **Superscript** | |
| $'$ | differentiation with respect to $\eta$ |

## References


1. Attia, H.A. Steady three-dimensional hydromagnetic stagnation point flow towards a stretching sheet with heat generation. *Ital. J. Pure Appl. Math.* **2010**, *2010*, 9–18.
2. Nazar, R.; Amin, N.; Pop, I. Unsteady boundary layer flow due to a stretching surface in a rotating fluid. *Mech. Res. Commun.* **2004**, *31*, 121–128. [CrossRef]
3. Shahid, A.; Huang, H.; Bhatti, M.M.; Zhang, L.; Ellahi, R. Numerical investigation on the swimming of gyrotactic microorganisms in nanofluids through porous medium over a stretched surface. *Mathematics* **2020**, *8*, 380. [CrossRef]
4. Vafai, K.; Khan, A.A.; Fatima, G.; Sait, S.M.; Ellahi, R. Dufour, Soret and radiation effects with magnetic dipole on Powell-Eyring fluid flow over a stretching sheet. *Int. J. Numer. Methods Heat Fluid Flow* **2021**, *31*, 1085–1103. [CrossRef]
5. Sears, W.R.; Telionis, D.P. Boundary-layer separation in unsteady flow. *SIAM J. Appl. Math.* **1975**, *28*, 215–235. [CrossRef]
6. Schlichting, H.; Gersten, K. *Boundary-Layer Theory*; Springer: Berlin/Heidelberg, Germany, 2016; ISBN 9783662529195.
7. Liao, S. Unsteady boundary-layer flows. In *Homotopy Analysis Method in Nonlinear Differential Equations*; Springer: Berlin/Heidelberg, Germany, 2012; pp. 403–421.

8. Suali, M.; Nik Long, N.M.A.; Ariffin, N.M. Unsteady stagnation point flow and heat transfer over a stretching/shrinking sheet with suction or injection. *J. Appl. Math.* **2012**, *2012*, 781845. [CrossRef]
9. Mukhopadhyay, S.; Andersson, H.I. Effects of slip and heat transfer analysis of flow over an unsteady stretching surface. *Heat Mass Transf. Stoffuebertragung* **2009**, *45*, 1447–1452. [CrossRef]
10. Nadeem, S.; Hussain, M.; Naz, M. MHD stagnation flow of a micropolar fluid through a porous medium. *Meccanica* **2010**, *45*, 869–880. [CrossRef]
11. Mukhopadhyay, S.; De, P.R.; Bhattacharyya, K.; Layek, G.C. Casson fluid flow over an unsteady stretching surface. *Ain Shams Eng. J.* **2013**, *4*, 933–938. [CrossRef]
12. Naganthran, K.; Nazar, R.; Pop, I. Unsteady stagnation-point flow and heat transfer of a special third grade fluid past a permeable stretching/shrinking sheet. *Sci. Rep.* **2016**, *6*, 24632. [CrossRef]
13. Bachok, N.; Ishak, A.; Pop, I. Unsteady boundary-layer flow and heat transfer of a nanofluid over a permeable stretching/shrinking sheet. *Int. J. Heat Mass Transf.* **2012**, *55*, 2102–2109. [CrossRef]
14. Soid, S.K.; Ishak, A.; Pop, I. Unsteady MHD flow and heat transfer over a shrinking sheet with ohmic heating. *Chin. J. Phys.* **2017**, *55*, 1626–1636. [CrossRef]
15. Dzulkifli, N.F.; Bachok, N.; Yacob, N.A.; Arifin, N.M.; Rosali, H. Unsteady stagnation-point flow and heat transfer over a permeable exponential stretching/shrinking sheet in nanofluid with slip velocity effect: A stability analysis. *Appl. Sci.* **2018**, *8*, 2172. [CrossRef]
16. Khan, U.; Waini, I.; Ishak, A.; Pop, I. Unsteady hybrid nanofluid flow over a radially permeable shrinking/stretching surface. *J. Mol. Liq.* **2021**, *331*, 115752. [CrossRef]
17. Childs, P.R.N. Rotating Flow. In *Rotating Cylinders, Annuli, and Spheres*; Elsevier Inc.: Amsterdam, The Netherlands, 2011; pp. 177–247. ISBN 9780123820983.
18. Anuar, N.S.; Bachok, N.; Pop, I. Radiative hybrid nanofluid flow past a rotating permeable stretching/shrinking sheet. *Int. J. Numer. Methods Heat Fluid Flow* **2020**, *31*, 914–932. [CrossRef]
19. Kármán, T.V. Über laminare und turbulente Reibung. *ZAMM J. Appl. Math. Mech. Zeitschrift Angew. Math. Mech.* **1921**, *1*, 233–252. [CrossRef]
20. Wang, C.Y. Stretching a surface in a rotating fluid. *ZAMP Zeitschrift Angew. Math. Phys.* **1988**, *39*, 177–185. [CrossRef]
21. Rajeswari, V.; Nath, G. Unsteady flow over a stretching surface in a rotating fluid. *Int. J. Eng. Sci.* **1992**, *30*, 747–756. [CrossRef]
22. Takhar, H.S.; Chamkha, A.J.; Nath, G. Flow and heat transfer on a stretching surface in a rotating fluid with a magnetic field. *Int. J. Therm. Sci.* **2003**, *42*, 23–31. [CrossRef]
23. Yacob, N.A.; Dzulkifli, N.F.; Nur, S.; Salleh, A.; Ishak, A. Rotating flow in a nanofluid with CNT nanoparticles over a stretching/shrinking surface. *Mathematics* **2022**, *10*, 7. [CrossRef]
24. Rana, P.; Bhargava, R.; Bég, O.A. Finite element simulation of unsteady magneto-hydrodynamic transport phenomena on a stretching sheet in a rotating nanofluid. *Proc. Inst. Mech. Eng. Part N J. Nanoeng. Nanosyst.* **2013**, *227*, 77–99. [CrossRef]
25. Maqsood, N.; Mustafa, M.; Khan, J.A. Numerical tackling for viscoelastic fluid flow in rotating frame considering homogeneous-heterogeneous reactions. *Results Phys.* **2017**, *7*, 3475–3481. [CrossRef]
26. Hayat, T.; Nadeem, S.; Khan, A.U. Rotating flow of Ag-CuO/H2O hybrid nanofluid with radiation and partial slip boundary effects. *Eur. Phys. J. E* **2018**, *41*, 75. [CrossRef] [PubMed]
27. Tassaddiq, A.; Khan, S.; Bilal, M.; Gul, T.; Mukhtar, S.; Shah, Z.; Bonyah, E. Heat and mass transfer together with hybrid nanofluid flow over a rotating disk. *AIP Adv.* **2020**, *10*, 055317. [CrossRef]
28. Choi, S.U.S.; Eastmen, J.A. Enhancing thermal conductivity of fluids with nanoparticles. In Proceedings of the Conference: 1995 International Mechanical Engineering Congress and Exhibition, San Francisco, CA, USA, 12–17 November 1995.
29. Uddin, M.J.; Sohail, A.; Bég, O.A.; Ismail, A.I.M. Numerical solution of MHD slip flow of a nanofluid past a radiating plate with Newtonian heating: A Lie group approach. *Alex. Eng. J.* **2018**, *57*, 2455–2464. [CrossRef]
30. Zulkifli, S.N.; Sarif, N.M.; Salleh, M.Z.; Azmi, E.F. MHD stagnation point flow of micropolar nanofluid with Soret and Dufour effects. *J. Phys. Conf. Ser.* **2019**, *1366*, 012015. [CrossRef]
31. Ghadimi, A.; Saidur, R.; Metselaar, H.S.C. A review of nanofluid stability properties and characterization in stationary conditions. *Int. J. Heat Mass Transf.* **2011**, *54*, 4051–4068. [CrossRef]
32. Noor, N.F.M.; Haq, R.U.; Nadeem, S.; Hashim, I. Mixed convection stagnation flow of a micropolar nanofluid along a vertically stretching surface with slip effects. *Meccanica* **2015**, *50*, 2007–2022. [CrossRef]
33. Ahmad, A.; Asghar, S.; Afzal, S. Flow of nanofluid past a Riga plate. *J. Magn. Magn. Mater.* **2016**, *402*, 44–48. [CrossRef]
34. Khan, U.; Zaib, A.; Ishak, A. Magnetic field effect on Sisko fluid flow containing gold nanoparticles through a porous curved surface in the presence of radiation and partial slip. *Mathematics* **2021**, *9*, 921. [CrossRef]
35. Devi, S.S.U.; Devi, S.P.A. Heat transfer enhancement of Cu−Al2O3/water hybrid nanofluid flow over a stretching sheet. *J. Niger. Math. Soc.* **2017**, *36*, 419–433.
36. Suresh, S.; Venkitaraj, K.P.; Selvakumar, P.; Chandrasekar, M. Synthesis of Al2O3-Cu/water hybrid nanofluids using two step method and its thermo physical properties. *Colloids Surf. A Physicochem. Eng. Asp.* **2011**, *388*, 41–48. [CrossRef]
37. Suresh, S.; Venkitaraj, K.P.; Selvakumar, P.; Chandrasekar, M. Effect of Al 2O 3-Cu/water hybrid nanofluid in heat transfer. *Exp. Therm. Fluid Sci.* **2012**, *38*, 54–60. [CrossRef]

38. Devi, S.S.U.; Devi, S.P.A. Numerical investigation of three-dimensional hybrid Cu-Al2O3/water nanofluid flow over a stretching sheet with effecting Lorentz force subject to Newtonian heating. *Can. J. Phys.* **2016**, *94*, 490–496. [CrossRef]
39. Waini, I.; Ishak, A.; Pop, I. Unsteady flow and heat transfer past a stretching/shrinking sheet in a hybrid nanofluid. *Int. J. Heat Mass Transf.* **2019**, *136*, 288–297. [CrossRef]
40. Waini, I.; Ishak, A.; Pop, I. Hybrid nanofluid flow and heat transfer over a permeable biaxial stretching/shrinking sheet. *Int. J. Numer. Methods Heat Fluid Flow* **2019**, *30*, 3497–3513. [CrossRef]
41. Waini, I.; Ishak, A.; Pop, I. Hybrid nanofluid flow towards a stagnation point on an exponentially stretching/shrinking vertical sheet with buoyancy effects. *Int. J. Numer. Methods Heat Fluid Flow* **2020**, *31*, 216–235. [CrossRef]
42. Waini, I.; Ishak, A.; Pop, I. MHD flow and heat transfer of a hybrid nanofluid past a permeable stretching/shrinking wedge. *Appl. Math. Mech.* **2020**, *41*, 507–520. [CrossRef]
43. Waini, I.; Ishak, A.; Pop, I. Hybrid nanofluid flow over a permeable non-isothermal shrinking surface. *Mathematics* **2021**, *9*, 538. [CrossRef]
44. Zainal, N.A.; Nazar, R.; Naganthran, K.; Pop, I. Unsteady three-dimensional MHD non-axisymmetric homann stagnation point flow of a hybrid nanofluid with stability analysis. *Mathematics* **2020**, *8*, 784. [CrossRef]
45. Hayat, T.; Nadeem, S. Heat transfer enhancement with Ag–CuO/water hybrid nanofluid. *Results Phys.* **2017**, *7*, 2317–2324. [CrossRef]
46. Khan, U.; Zaib, A.; Pop, I.; Abu Bakar, S.; Ishak, A. Stagnation point flow of a micropolar fluid filled with hybrid nanoparticles by considering various base fluids and nanoparticle shape factors. *Int. J. Numer. Methods Heat Fluid Flow* **2022**. [CrossRef]
47. Takabi, B.; Salehi, S. Augmentation of the heat transfer performance of a sinusoidal corrugated enclosure by employing hybrid nanofluid. *Adv. Mech. Eng.* **2014**, *2014*, 147059. [CrossRef]
48. Oztop, H.F.; Abu-Nada, E. Numerical study of natural convection in partially heated rectangular enclosures filled with nanofluids. *Int. J. Heat Fluid Flow* **2008**, *29*, 1326–1336. [CrossRef]
49. Bataller, R.C. Radiation effects for the Blasius and Sakiadis flows with a convective surface boundary condition. *Appl. Math. Comput.* **2008**, *206*, 832–840. [CrossRef]
50. Ishak, A. Thermal boundary layer flow over a stretching sheet in a micropolar fluid with radiation effect. *Meccanica* **2010**, *45*, 367–373. [CrossRef]
51. Magyari, E.; Pantokratoras, A. Note on the effect of thermal radiation in the linearized Rosseland approximation on the heat transfer characteristics of various boundary layer flows. *Int. Commun. Heat Mass Transf.* **2011**, *38*, 554–556. [CrossRef]
52. Roşca, N.C.; Roşca, A.V.; Pop, I. Axisymmetric flow of hybrid nanofluid due to a permeable non-linearly stretching/shrinking sheet with radiation effect. *Int. J. Numer. Methods Heat Fluid Flow* **2020**, *31*, 2330–2346. [CrossRef]
53. Fang, T.G.; Zhang, J.; Yao, S.S. Viscous flow over an unsteady shrinking sheet with mass transfer. *Chin. Phys. Lett.* **2009**, *26*, 014703. [CrossRef]
54. Shampine, L.F.; Gladwell, I.; Thompson, S. *Solving ODEs with MATHLAB*; Cambridge University Press: Cambridge, UK, 2003; ISBN 9780521824040.